,

Supplement for: A data-calibrated distribution of deglacial chronologies for the North American ice complex from glaciological modeling

Lev Tarasov[a,*], Arthur S. Dyke[b], Radford M. Neal[c], W. R. Peltier[d]

[a] *Department of Physics and Physical Oceanography, Memorial University of Newfoundland and Labrador, St. John's, Canada, A1B 3X7*
[b] *Geological Survey of Canada, Ottawa, Canada, K1A 0E8*
[c] *Department of Physics, University of Toronto, Toronto, Canada, M5S 1A7*
[d] *Department of Statistics and Department of Computer Science, University of Toronto, Toronto, Canada, M5S 3G3*

1. Ensemble parameters

We here briefly document the expansion and change in the set of ensemble parameters relative to Tarasov and Peltier (2004). The whole set of ensemble parameters is listed in Tables 1 and 2. The descriptions below refer to the parameter names in that table (which correspond primarily to the actual names used in the model Fortran code, except for those listed in italics which follow the usage set forth in Tarasov and Peltier (2004))

A key change in the climate forcing is that there is now explicit topographic control for climate re-organization. For maximum Keewatin ice surface elevation below 1 km, PMIP I mean fields for LGM (which used the ICE4-G ice load reconstruction that lacked a Keewatin ice-dome as a boundary condition) and the des0 desert-elevation factor are used. Above 2km, PMIP II fields (which used the ICE5-G reconstruction with large Keewatin ice dome) are used along with the suite of desert elevation parameters which we posit might crudely account for atmospheric reorganization due to the presence of the Keewatin ice dome. Between 1 and 2km, the relevant fields are interpolated according to a power law under the control of the rtdes parameter.

The set of regional desert elevation parameters has been expanded to provide more regional control in the calibration. These parameters set the threshold above which the vertical gradient in precipitation strongly decreases (*i.e.* strong increase in the rate of reduction with elevation). Furthermore, the threshold elevations are now relative to the surface elevation used for the PMIP boundary conditions (with interpolation between

*Ph: 1-709-864-2675, Fax: 1-709-864-8739,
Email address: `lev@mun.ca` (Lev Tarasov)
URL: `http://www.physics.mun.ca/~lev/` (Lev Tarasov)

Table 1: Non-climate forcing ensemble parameters

Definition	Parameter	Range
linear Weertman parameter for till	rmu	$1.5 \times 10^{-2} \rightarrow 0.4$ m/yr Pa^{-1}
sliding parameter	fnslid	$0.4 \times 10^{-13} \rightarrow 18.0 \times 10^{-13}$ m/yr Pa^{-3}
marine till enhancement factor	rmmf	$1.0 \rightarrow 3.0$
ice shelf Weertman parameter	dsb	$50 \rightarrow 740$ m/yr Pa$^{-0.5}$
pre-Heinrich till parameter reduction	rHEtillmn	$1.0 \rightarrow 1.0 \times 10^{-5}$
maximum calving velocity	U_{Cmx}	$0.05 \rightarrow 2.5$ km/yr
summer temperature calving cut-in	T_{mn}	$-6 \rightarrow 0^oC$
regional NW maximum calving velocity	U_{CNWmx}	$0.1 \rightarrow 2.4$ km/yr
lacustrine calving parameter	flac	$0. \rightarrow 0.4$
margin chronology weighting	wmargw	$0 \rightarrow 1.0$
margin forcing ablation threshold	margab	$1.1 \rightarrow 1.99$
margin forcing accumulation threshold	margac	margab $+0. \rightarrow 0.9$
primary margin forcing accum. threshold	faccut	$400 \rightarrow 800$ m
margin forcing calving reduction factor	margcalv	$0. \rightarrow 1.$
margin forcing initiation time	fmgpin	$23.35 \rightarrow 30ka$

ICE4-G and ICE5-G as required if the maximum elevation of the Keewatin ice dome is between 1 and 2 km).

The Keewatin precipitation factor (fnpreW) now controls a slope-dependent enhancement of precipitation to represent orographic forcing of precipitation.

The other major addition is that Heinrich events 1 and 2 are dynamically facilitated by a reduction in the Weertman till parameter (by a factor equal to the "rHEtillmin" ensemble calibration parameter) for Hudson strait during the 27.1 to 24.0 ka and 19.6 to 17.1 ka intervals preceding these events. A much weaker precursor reduction is also applied during the 29.0 to 27.1 ka interval (again controlled by 'rHEtillmin").

The margin forcing threshold ensemble parameters indicate at what value of the margin raster zone (interpolated between time-slices) the forcing should smoothly activate. The primary margin forcing accumulation threshold (faccut) is the elevation below which positive surface mass-balance is enforced for raster zone values above the margin forcing accumulation threshold. The margin chronology weighting parameter (wmargw) controls the weighting between a margin chronology with narrow error bars (maximum ± 500 years) versus the standard set as described in the main text.

Those desiring additional details are welcome to contact the corresponding author.

Table 2: Climate forcing ensemble parameters

Definition	Parameter	Range
global LGM precipitation scale factor	fnpre	$0.8 \rightarrow 1.4$
Keewatin precipitation factor	fnpreW	$1.0 \rightarrow 3.5$
South central precipitation enhancement	fmpreSM	$0. \rightarrow 1.0$
precipitation phase factor	Θ_P	$0.5 \rightarrow 2.5$
desert elevation control parameter	rtdes	$0. \rightarrow 1.$
non-glacial desert-elevation cutoff	des0	$0.4 \rightarrow 2.2$ km
western desert-elevation cutoff	desW	$0.2 \rightarrow 3.0$ km
northwestern desert-elevation cutoff	desNW	$0. \rightarrow 2.0$ km
north-central desert-elevation cutoff	desNC	$0. \rightarrow 1.5$ km
central desert-elevation cutoff	desC	$0. \rightarrow 2.0$ km
Foxe Basin/Baffin desert-elevation cutoff	desF	$0. \rightarrow 2.0$ km
Quebec/Labrador desert-elevation cutoff	desQ	$0. \rightarrow 2.2$ km
mid-south-central desert-elevation cutoff	desScN	$0. \rightarrow 2.4$ km
south-central desert-elevation cutoff	desSC	$0. \rightarrow 1.0$ km
remainder desert-elevation cutoff	des2	$0. \rightarrow 2.$ km
LGM Southern Hudson Bay precip. enhancement	fsHb	$0. \rightarrow 2.0^oC$
2 LGM precipitation EOF components	fPEOF[2]	150% of PMIP range
1 LGM evaporation EOF component	fEEOF[1]	150% of PMIP range
global LGM temperature scale factor	fnT	$0.85 \rightarrow 1.2$
Environmental lapse rate	desC	$4.0 \rightarrow 8.0^oC/$ km
2 LGM temperature EOF components	fTEOF[2]	150% of PMIP range
LGM Southern Hudson Bay temperature enhancement	fsHbT	$0. \rightarrow 2.0^oC$

Table 3: GSM input data sets

component	data source	main direct impact
present day precipitation	observed climatology (Legates and Willmott, 1990)	
present day temperature	Reanalysis data set (Kalnay et al., 1996)	
LGM precipitation	PMIP I & II ensembles	ice geometry
LGM temperature	PMIP I $ II ensembles	” ” and pre-LGM margin location
climate interpolation	glaciological inversion of GRIP $\delta^{18}O$ (Tarasov and Peltier, 2002)	” ” and meltwater flux
sediment map for till deformation	derived from sediment map (Laske and Masters, 1997)	ice geometry
	and surficial geology map (Fulton, 1995)	
deep geothermal heat flux	map of Pollack et al. (1993)	ice geometry and basal melt
earth radial viscosity	VM2 (Peltier, 1996; Peltier and Jiang, 1996)	ice geometry & surface drainage routing
earth radial elasticity	PREM model (Dziewonski and Anderson, 1981)	
eustatic sea level chronology	Fairbanks (1989); Peltier and Fairbanks (2006),Waelbroeck et al. (2002)	marine ice margin & coastal inundation

2. GSM input data sets

Table 3 provides a brief summary of the input data sets used in the GSM.

3. Mwp1a and 20ka ice volumes versus metric components

Comparisons between metric score components and 20 ka ice volumes are shown in Figs. 1 and 2. These plots show the general agreement in best-fit volume range under the cut3M data-sieve (with Rdot offering the weakest constraint on the upper bound). Also worth noting is the extent of probing over a large range of ice volumes as shown in the latter plot.

Similar comparisons with mwp1 contributions are shown in Figs. 3 and 4. 3 and 4.

4. Example fits to constraint data

Sample strandline elevation fits of model predictions are shown in Table 4. When evaluating the level of fit, one should consider the relatively coarse resolution of the model compared to the scale of strandline elevation variation. Strandlines for southern Lake Agassiz are controlled by imposed time-dependent changes to the elevation of the sill for the southern outlet as detailed in Tarasov and Peltier (2006). However, the sill elevation chronology has since been updated as follows. As before, it is initially set to 332 m. Upon overflow after 13.95 ka, sill elevation is reduced to 316 m. Upon

Table 4: Comparison of GSM strandline predictions (masl) against values inferred from observations. Run nn9927 has one of the best overall scores. nn9894 has a bit weaker overall score and deglaciates Hudson Bay too early (figure 12 in the tertiary supplement) but it has a better strandline score, while nn9390 has an even better strandline score but doesn't pass the 20 and 26 ka volume constraints (nn9390 has 67.9 mESL at 20ka). Sites are abbreviated as follows. Certain site locations were slightly adjusted from source values to better correspond to model grid-cell location. Equality of strandline values between different model runs indicate lake transgression of the site during the data-window and interpolated grid-cell elevation is provided instead. The first 3 sites are from southern Lake Agassiz: SRR (Red River, 96.39^{o}W, 47.97^{o}N), SA2 (Lower Campbell, 96.7^{o}W, 46.1^{o}N), SAw(92.9^{o}W, 49.0^{o}N) (Fisher, 2005; Fisher et al., 2008; Teller et al., 2000). The following sites are from Smith (1994): GS1 Great Slave (112^{o}W, 62.42^{o}N), GB1 Great Bear (118.3^{o}W, 66.64^{o}N), LA1 Lake Athabasca (110.3^{o}W, 58.67^{o}N), MR1 Mountain River (128.9^{o}W, 65.65^{o}N), SI1 Fort Simpson (123.2^{o}W,62.18^{o}N), PD1/2 Peace River delta (113.0^{o}W, 58.95^{o}N), AD Athabasca delta (111.42^{o}W, 58.25^{o}N). The values for the following sites were the highest adjacent strandlines from Veillette (1994): VCh Chibougamau (74.35^{o}W, 49.87^{o}N), VMa Matagami (77.63^{o}W, 49.75^{o}N), VTe Lake Temiskaming (79.5^{o}W, 47.33^{o}N), VTm Timmins (81.33^{o}W, 48.47^{o}N), VAm Amos (78.12^{o}W, 48.57^{o}N). Site FS1 (107.95^{o}W, 56.18^{o}N) is below the Clearwater lower Athabasca Spillway (Fisher and Smith, 1994). The total logarithmic strandline score is given in the last column.

	SRR	SA2	SAw	GS1	GB1	LA1	MR1	SI1	PD1
obs.	302	298	362	320	298	315	87	122	235
nn9927	271	293	356	432	295	387	118	139	330
nn9894	271	293	356	450	295	374	118	133	315
nn9390	271	293	356	427	301	350	122	122	286

	PD2	AD1	VCh	VMa	VTe	VTm	VAm	FS1	score
obs.	215	228	445	462	330	365	409	490	
nn9927	269	343	393	462	342	398	463	603	1.826
nn9894	259	326	455	496	346	408	466	551	1.351
nn9390	245	304	445	468	336	381	441	581	1.228

overflow after 13.75 ka, it is reduced to 309 m. Subsequent reductions to 304 and 295 m occur upon overflow after 13.55 ka and 10.82 ka respectively.

Sample present-day vertical velocity fits of model runs to observations for higher weighted sites are given in Table 5. Aside from Sch (Schefferville), the 3 sample runs fit the given observations within source uncertainties.

A table of summary characteristics and scores for runs nn9927 and nn9894 is provided in the tertiary supplement. That supplement also includes a deglacial set of time-slice maps for those two runs.

Table 5: Sample of results for present day vertical velocities (mm/yr) for 8 of the top weighted sites. Site abbreviations follow convention from data source (Argus and Peltier, 2010). The total (ie for all 110 sites) logarithmic vertical velocity score is given in the last column. Runs nn9927 and nn9894 are described in Table 4. Run nn9627 has the best vertical velocity score but insufficient 20 and 26 ka ice volume (64.5 mESL at 20ka).

site	Yel	Chu	Fli	StJ	Alg	Kuu	Sch	Val	score
obs.	4.8	10.2	2.7	-1.1	1.8	10.0	9.8	5.2	
$\pm$	1.4	2.6	2.6	1.5	1.1	3.4	2.1	2.6	
nn9927	5.56	11.69	3.62	-0.89	1.47	12.67	13.80	4.84	0.337
nn9894	6.05	11.39	3.39	-0.21	1.65	11.98	13.55	5.10	0.329
nn9627	5.49	10.99	2.90	-0.73	1.68	14.59	10.92	3.93	0.239

5. Ensemble time-slices

Of perhaps particular interest is the regional pattern of mass-loss during mwp1-a as can be discerned from comparison of Figs. .8 and .9. The majority of mass-loss is from the western sector of the Laurentide ice sheet.

A feature in the set of displayed time-slices that may invoke reaction from the geological community is the large and persistent Patrician Dome over what is now Ontario. The sequence leaves only a brief late interval for onshore transport of carbonate drift from Hudson Bay/Lowlands onto the Canadian Shield (Dredge and Cowan, 1989) and suggests bay-ward flow for a long interval, largely warm-based, for which we lack evidence. This is a persistent feature in the GSM to due to the hard bed (Canadian Shield) north and northwest of Lake Superior.

References

Argus, D. F., Peltier, W. R., 2010. Constraining models of postglacial rebound using space geodesy: a detailed assessment of model ice-5g (vm2) and its relatives. Geophys. J. Int. 181, 697–732.

Dredge, L. A., Cowan, W. R., 1989. Quaternary geology of the southwestern Canadian Shield. In: Fulton, R. J. (Ed.), Quaternary Geology of Canada and Greenland. No. 1 in Geology of Canada. Geological Survey of Canada, pp. 214–249.

Dziewonski, A. M., Anderson, D. L., 1981. Preliminary reference Earth model. Phys. Earth Planet. Inter. 25, 297–356.

Fairbanks, R. G., 1989. A 17,000-year glacio-eustatic sea level record: influence of glacial melting rates on the Younger Dryas event and deep-ocean circulation. Nature 342, 637–641.

Fisher, T. G., 2005. Strandline analysis in the southern basin of glacial Lake Agassiz, Minnesota and North and South Dakota, USA. Geol. Soc. of America Bull. 117 (11/12), 1481–1496.

Fisher, T. G., Smith, D. G., 1994. Glacial Lake Agassiz - its northwest maximum extent and outlet in Saskatchewan (Emerson phase). Quat. Sci. Rev. 13 (9-10), 845–858.

Fisher, T. G., Yansa, C. H., Lowell, T. V., Lepper, K., Hajdas, I., Ashworth, A., JUN 2008. The chronology, climate, and confusion of the Moorhead Phase of glacial Lake Agassiz: new results from the Ojata Beach, North Dakota, USA. Quat. Sci. Rev. 27 (11-12), 1124–1135.

Fulton, R. J., 1995. Surficial materials of Canada, Geological Survey of Canada, Map 1880A, scale 1:5000000. online.

Kalnay, E., Kanamitsu, M., Kistler, R., Collins, W., Deaven, D., Gandin, L., Iredell, M., Saha, S., White, G., Woollen, J., Zhu, Y., Leetmaa, A., , Reynolds, B., Chelliah, M., Ebisuzaki, W., Higgins, W., Janowiak, J., Mo, K., Ropelewski, C., , Wang, J., Jenne, R., Joseph, D., 1996. The NCEP/NCAR 40-year reanalysis project. Bull. Amer. Met. Soc. 77, 437–471.

Laske, G., Masters, G., 1997. A global digital map of sediment thickness. EOS Trans. 78, F483.

Legates, D. R., Willmott, C. J., 1990. Mean seasonal and spatial variability in gauge-corrected global precipitation. Int. J. Climatol. 10 (2), 111–127.

Peltier, W. R., 1996. Mantle viscosity and ice age ice sheet topography. Science 273, 1359–1364.

Peltier, W. R., Fairbanks, F. G., 2006. Global glacial ice volume and last glacial maximum duration from an extended Barbados sea level record. Quat. Sci. Rev. 25, 3322–3337.

Peltier, W. R., Jiang, X., 1996. Mantle viscosity from the simultaneous inversion of multiple data sets pertaining to postglacial rebound. Geophys. Res. Lett. 23, 503–506.

Pollack, H. N., Hurter, S. J., Johnson, J. R., 1993. Heat flow from the Earth's interior: Analysis of the global data set. Rev. Geophys. 31, 267–280.

Smith, D. G., 1994. Glacial Lake McConnell: Paleogeography, age, duration, and associated river deltas, Mackenzie River basin, Western Canada. Quat. Sci. Rev. 13, 829–843.

Tarasov, L., Peltier, W. R., 2002. Greenland glacial history and local geodynamic consequences. Geophys. J. Int. 150, 198–229.

Tarasov, L., Peltier, W. R., 2004. A geophysically constrained large ensemble analysis of the deglacial history of the North American ice sheet complex. Quat. Sci. Rev. 23, 359–388.

Tarasov, L., Peltier, W. R., 2006. A calibrated deglacial drainage chronology for the North American continent: Evidence of an Arctic trigger for the Younger Dryas. Quat. Sci. Rev. 25 (7-8), 659–688.

Teller, J. T., Risberg, J., Matile, G., Zoltai, S., 2000. Postglacial history and paleoecology of Wampum, Manitoba, a former lagoon in the Lake Agassiz basin. Geol. Soc. of Amer. Bull. 112 (6), 943–958.

Veillette, J. J., 1994. Evolution and paleohydrology of glacial lakes Barlow and Ojibway. Quat. Sci. Rev. 13, 945–971.

Waelbroeck, C., Labeyrie, L., Michel, E., Duplessy, J., McManus, J., Lambeck, K., Balbon, E., Labracherie, M., 2002. Sea-level and deep water temperature changes derived from benthic foraminifera isotopic records. Quat. Sci. Rev. 21 (1-3), 295–305.

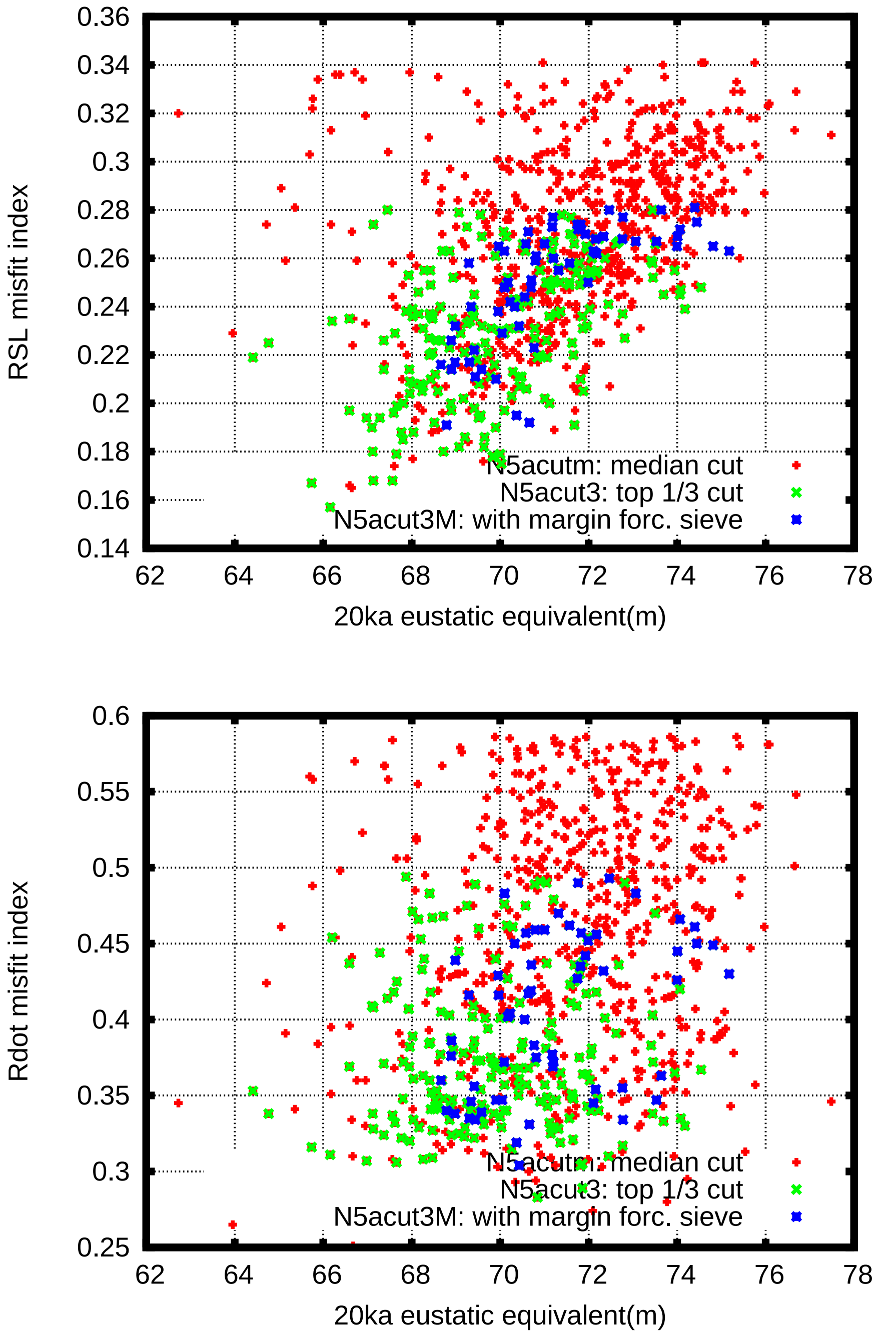

Figure 1: Ensemble member 20 ka eustatic equivalent ice volumes versus RSL and Rdot misfit indices (cost function values) for 3 sievings of the full ensemble. N5acutm only includes ensemble N5a runs that are better than median for each of the 4 main metric components (RSL, ML, Rdot, strandlines), that have final collapse of the Hudson Bay ice dome after 8.6 ka, and that have at least 0.5 dSv discharge of meltwater into the Gulf of Mexico during the 14.4 ka to 13.7 ka interval. The cut3 sieve is similar except that it only accepts runs in the top tertile for each main metric component. The cut3m sieve further imposes the filter of requiring below median margin forcing for each of the 6 margin forcing metric components. Neither filter imposes any ice volume or mwp1a contribution threshold.

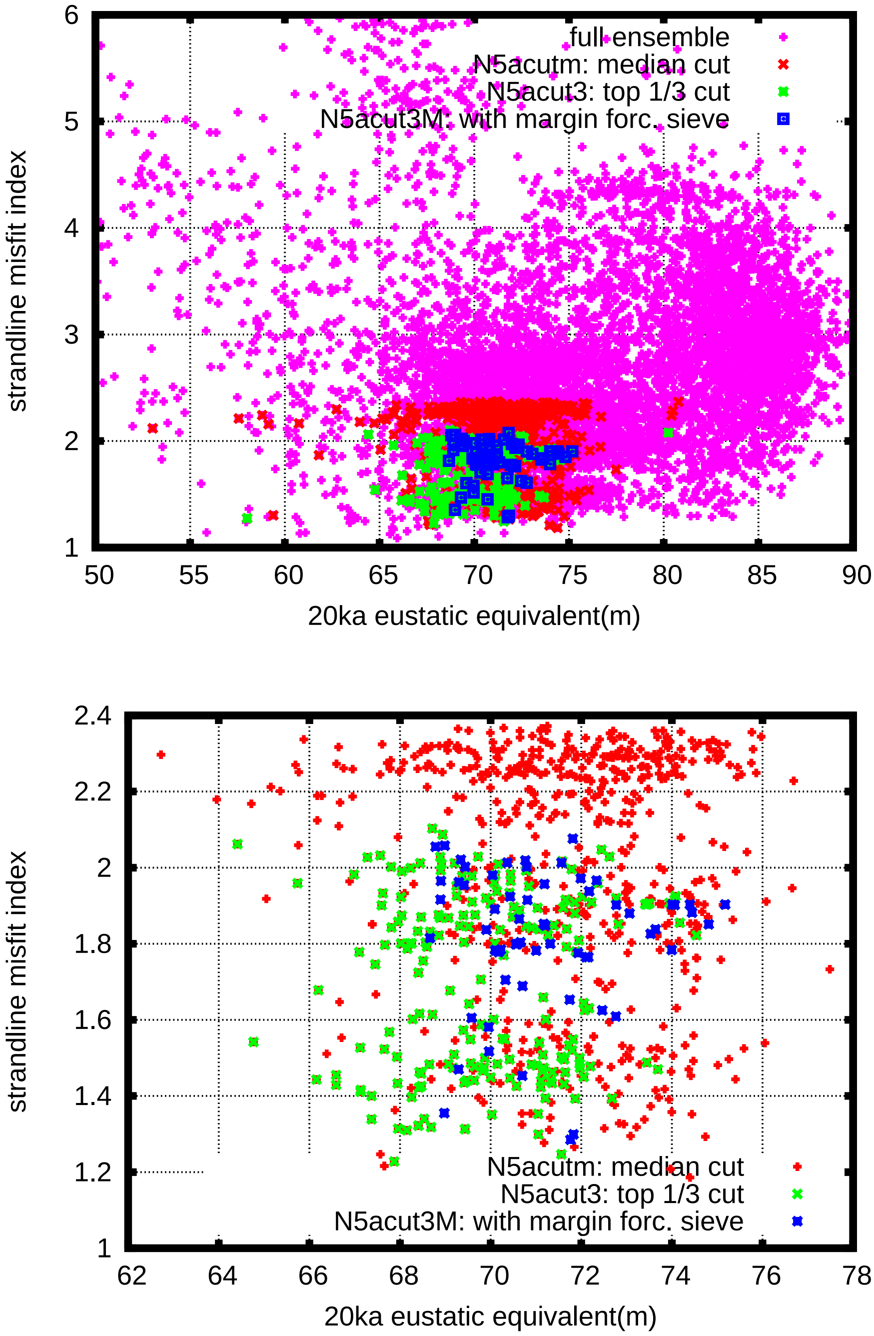

Figure 2: Ensemble member 20 ka eustatic equivalent ice volumes versus strandline misfit index (cost function value) for 3 sievings of the full ensemble.

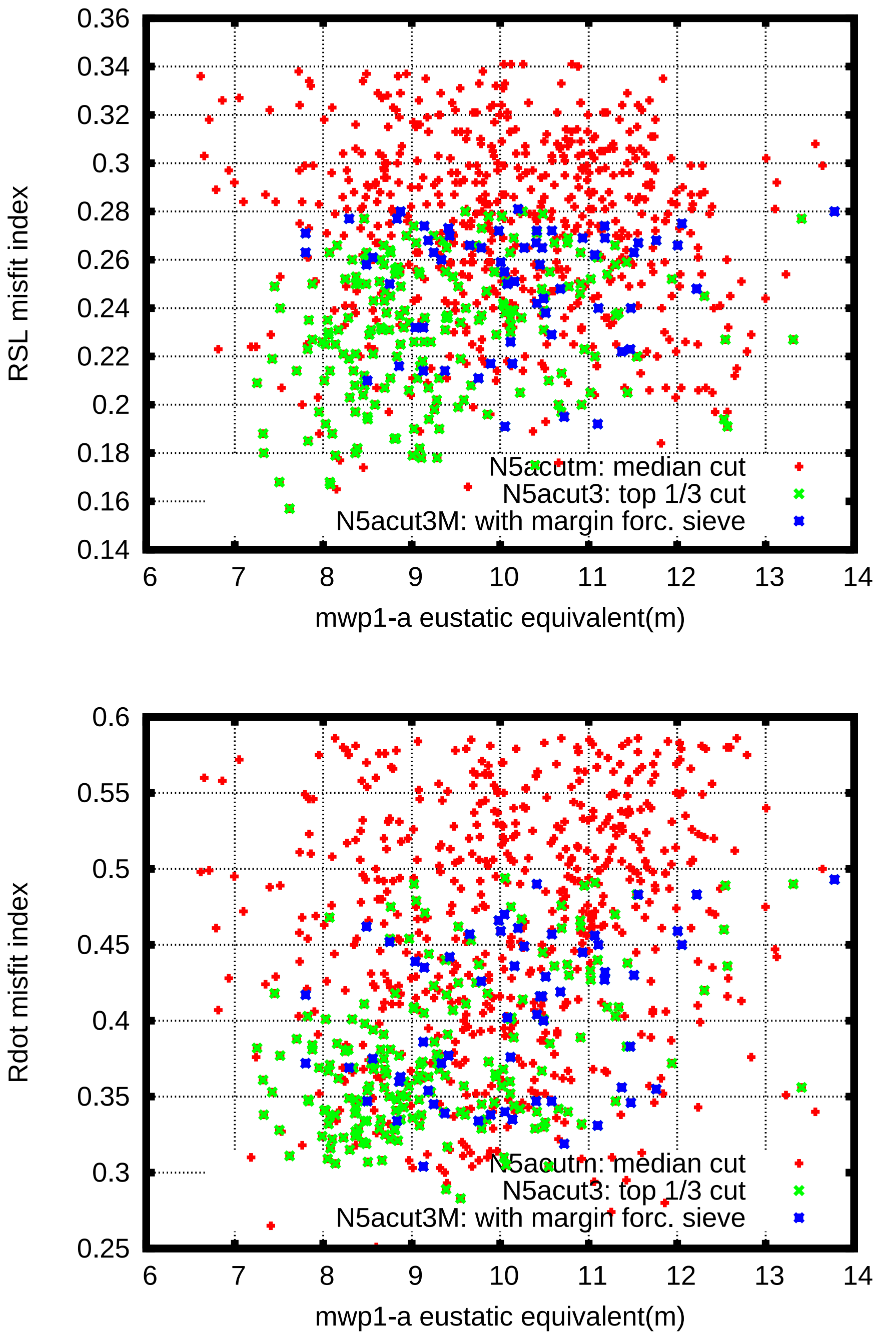

Figure 3: Ensemble member mwp1a contributions versus RSL and Rdot misfit indices (cost function values) for 3 sievings of the full ensemble.

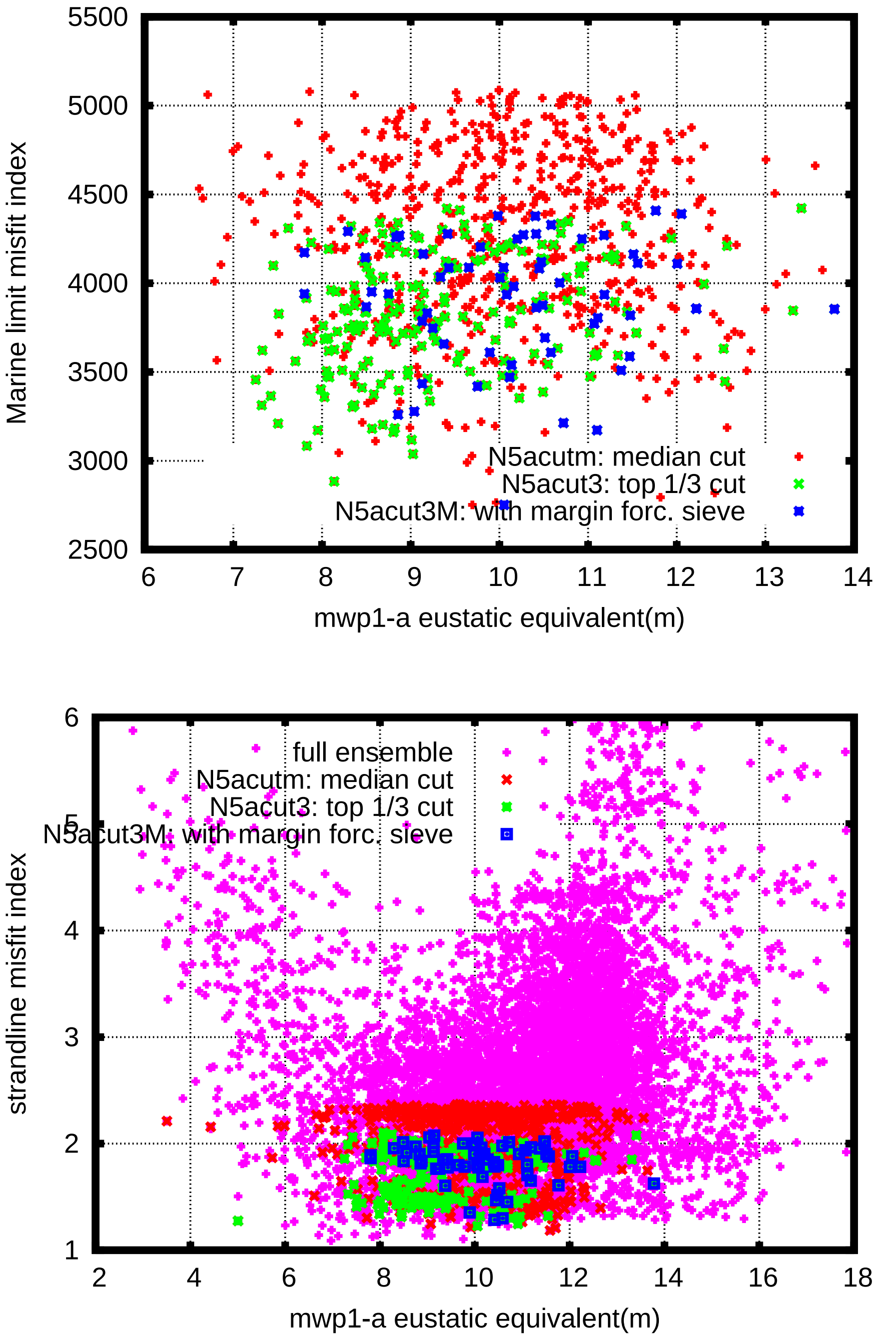

Figure 4: Ensemble member mwp1a contributions versus ML and strandline misfit indices (cost function values) for 3 sievings of the full ensemble.

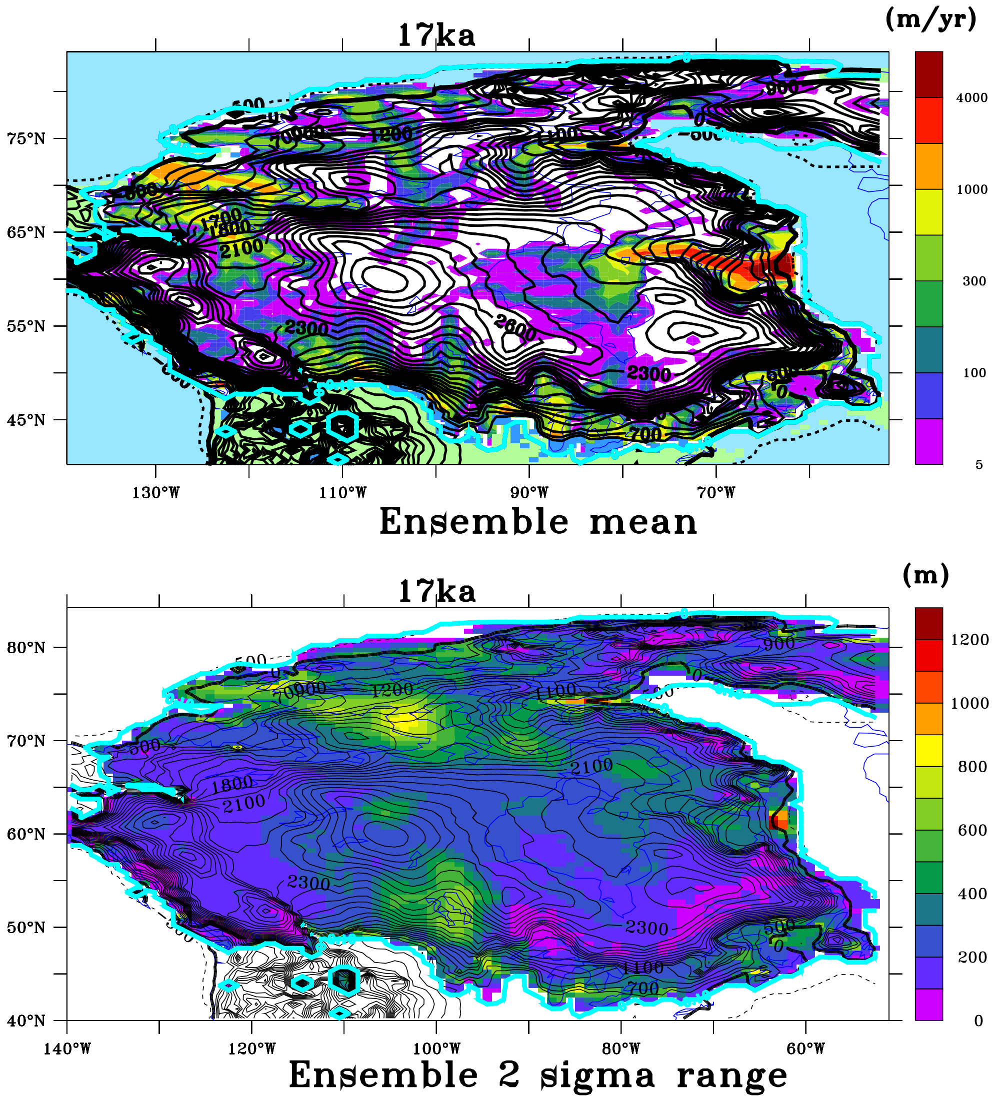

Figure .5: 17 ka weighted mean basal velocity and surface elevation for ensemble N5a and (one-way) two sigma range for ice thickness. Only lakes of depth greater than 10 m are shown in this and subsequent time-slice plots. Furthermore shorelines are those from the GSM and therefore do not take into account geoidal deformation (which is taken into account for RSL calculations).

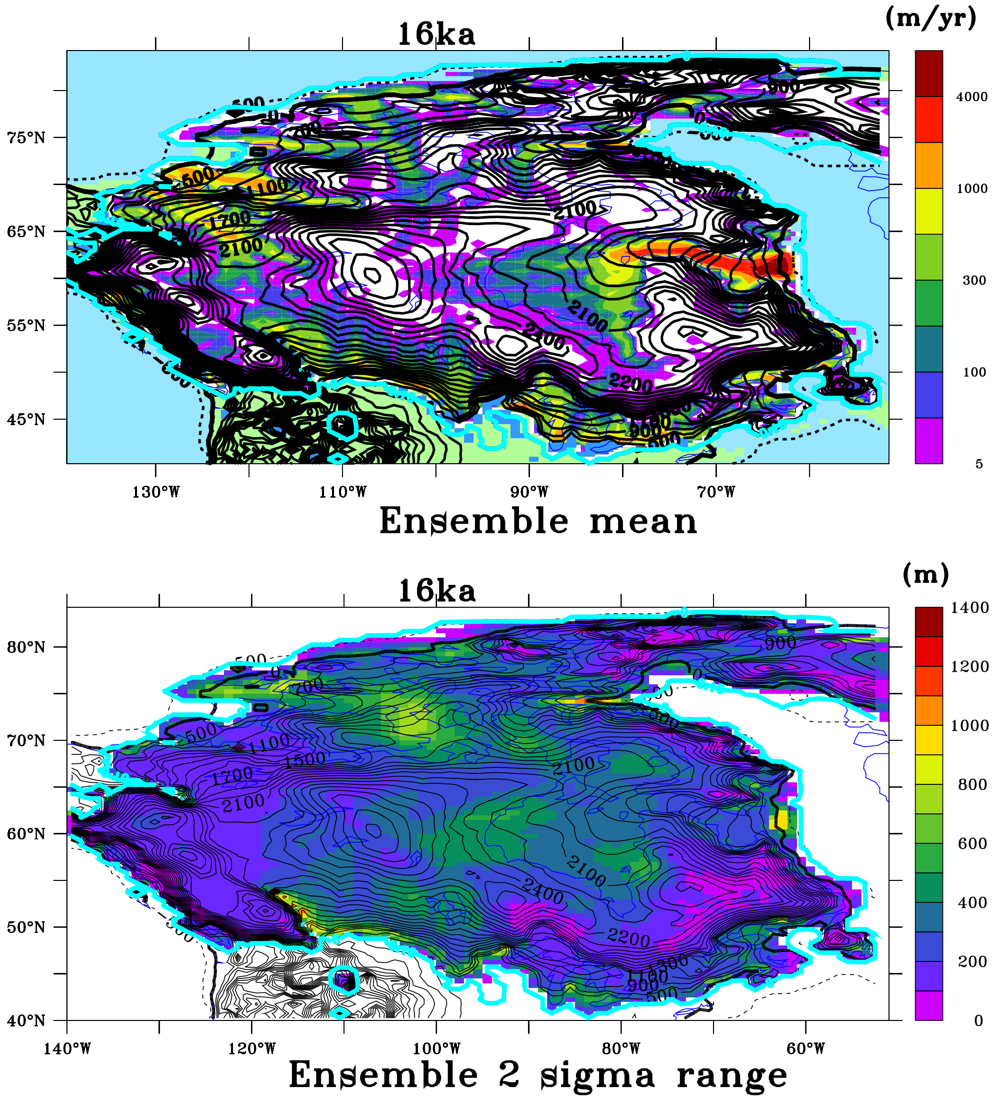

Figure .6: 16 ka weighted mean basal velocity and surface elevation for ensemble N5a and (one-way) two sigma range for ice thickness.

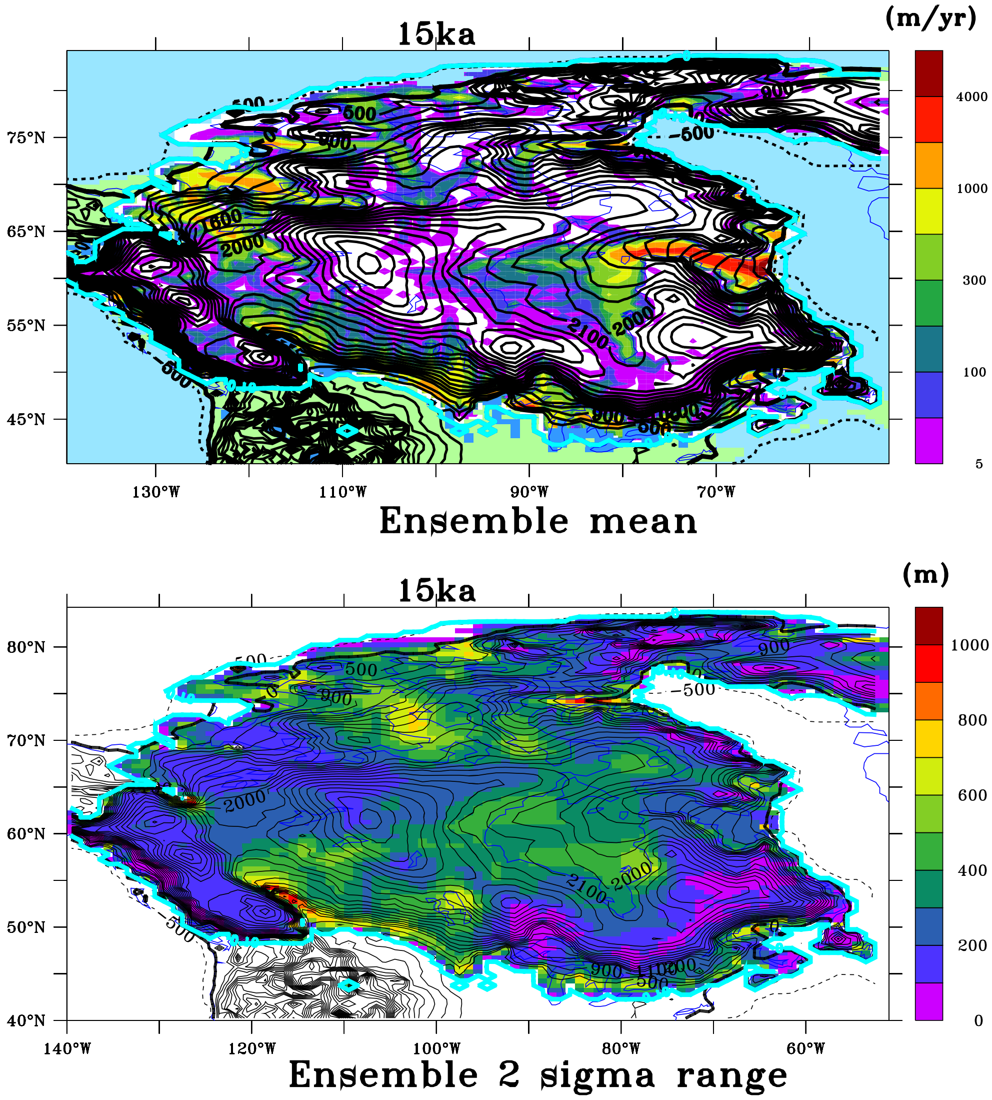

Figure .7: 15 ka weighted mean basal velocity and surface elevation for ensemble N5a and (one-way) two sigma range for ice thickness.

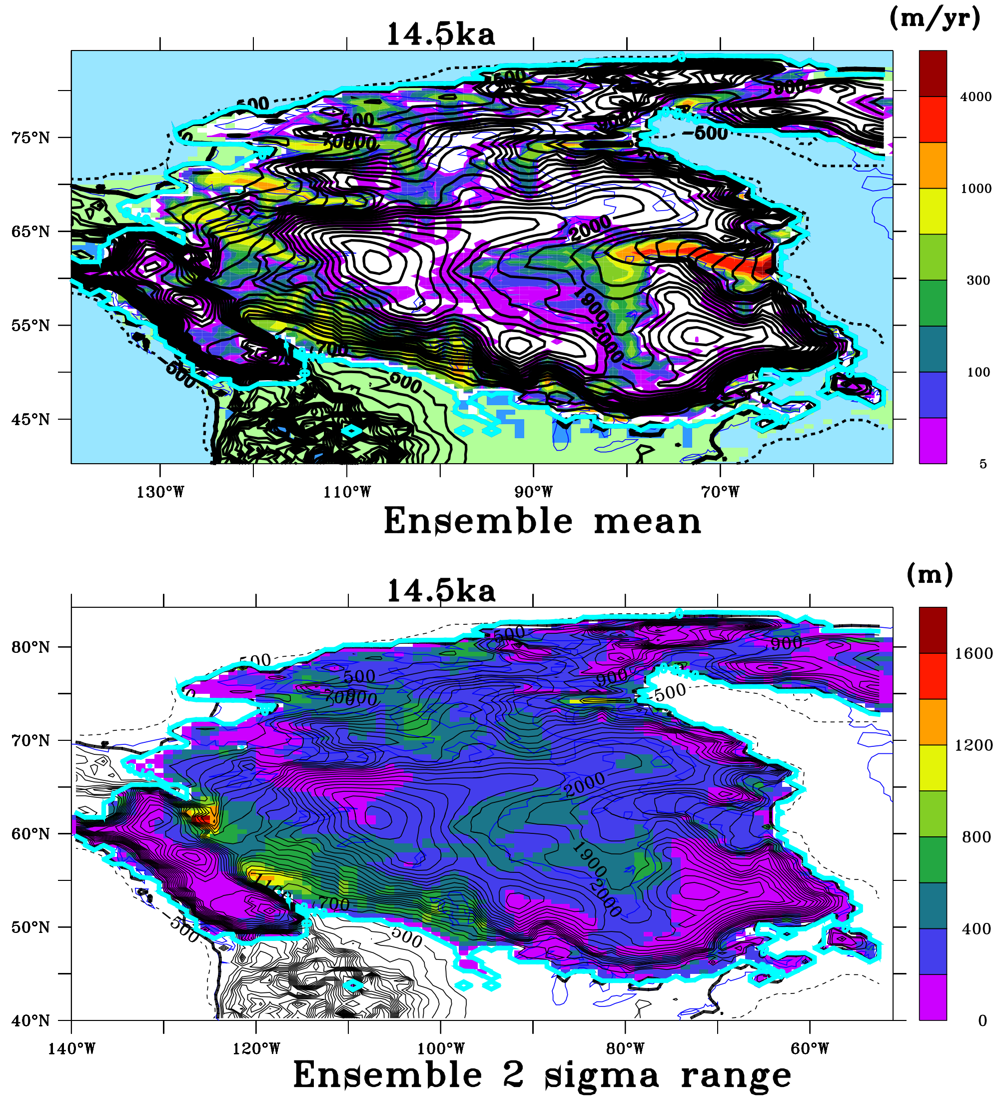

Figure .8: 14.5 ka weighted mean basal velocity and surface elevation for ensemble N5a and (one-way) two sigma range for ice thickness.

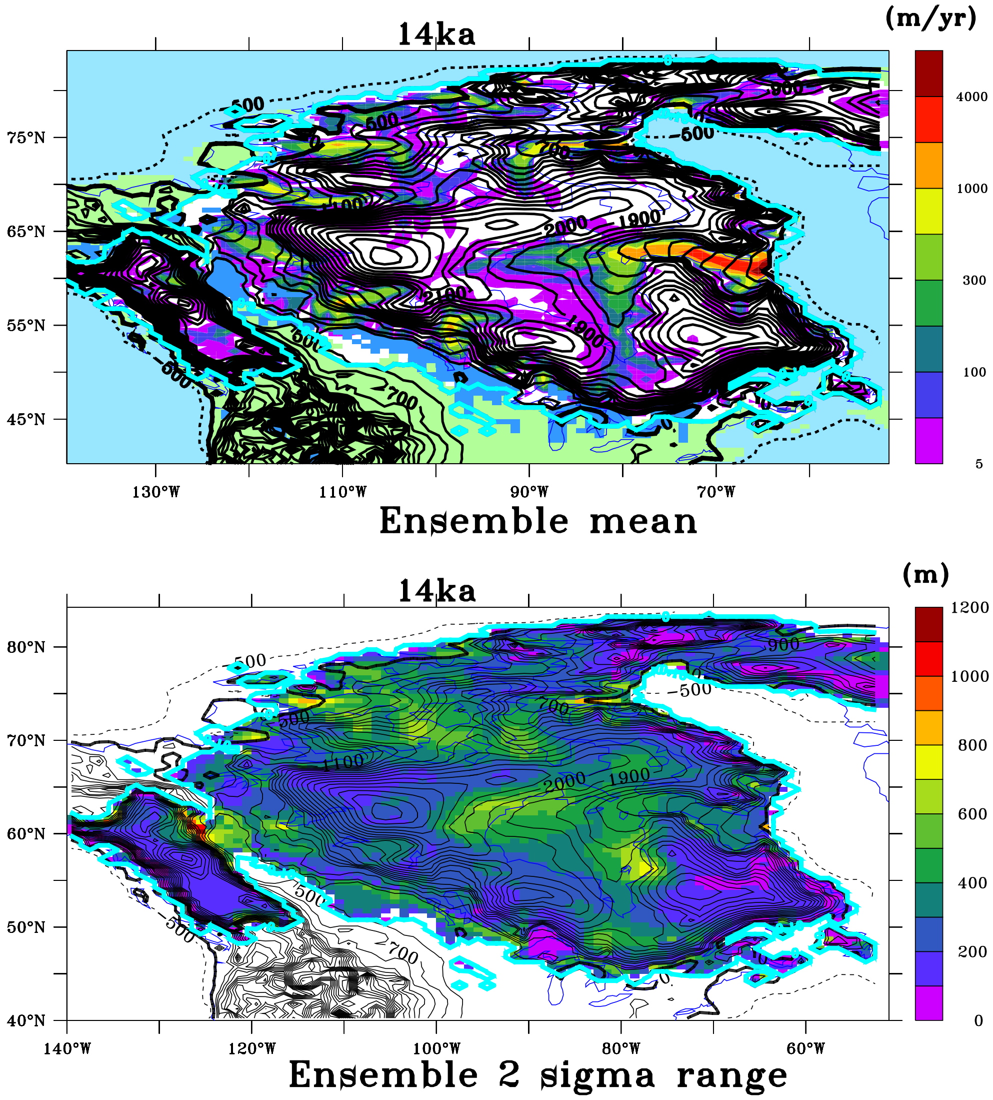

Figure .9: 14 ka weighted mean basal velocity and surface elevation for ensemble N5a and (one-way) two sigma range for ice thickness.

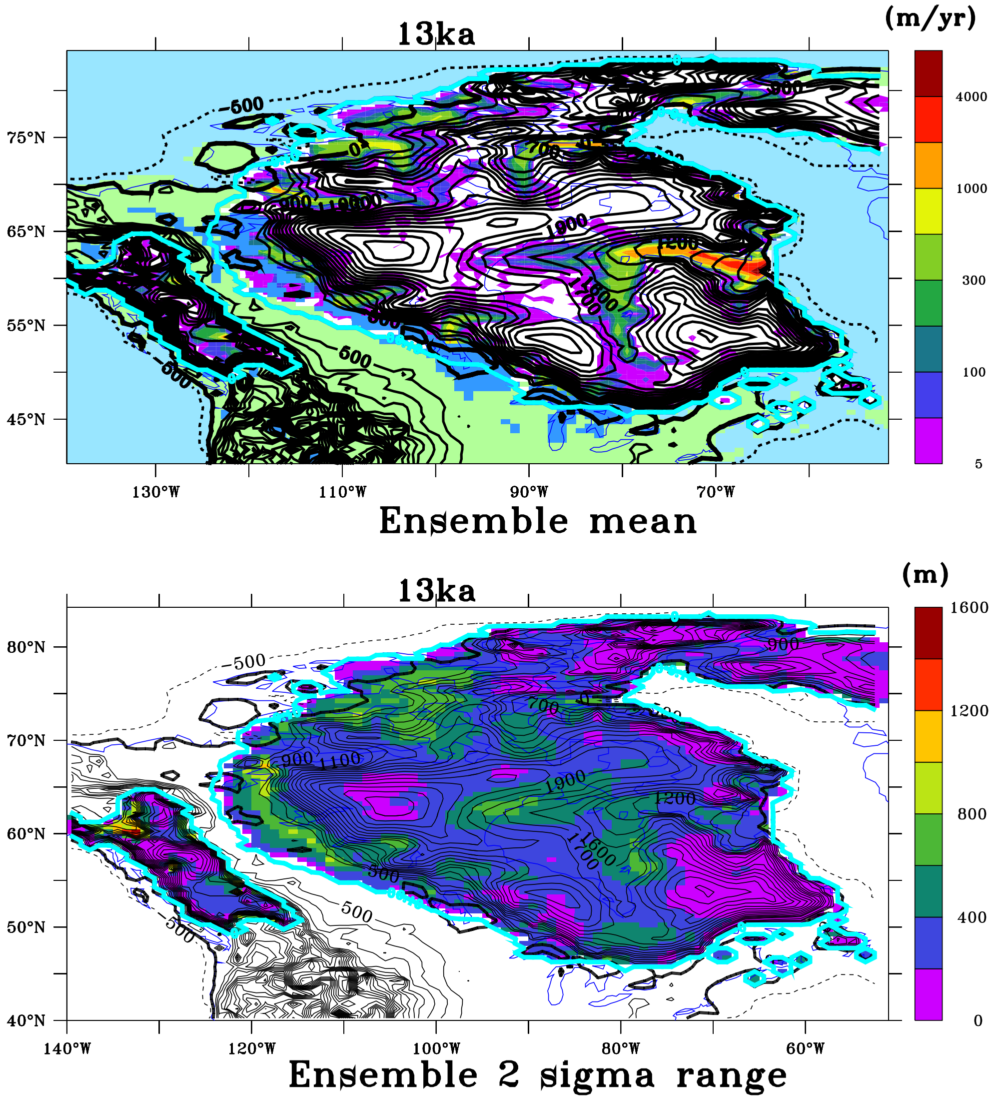

Figure .10: 13 ka weighted mean basal velocity and surface elevation for ensemble N5a and (one-way) two sigma range for ice thickness.

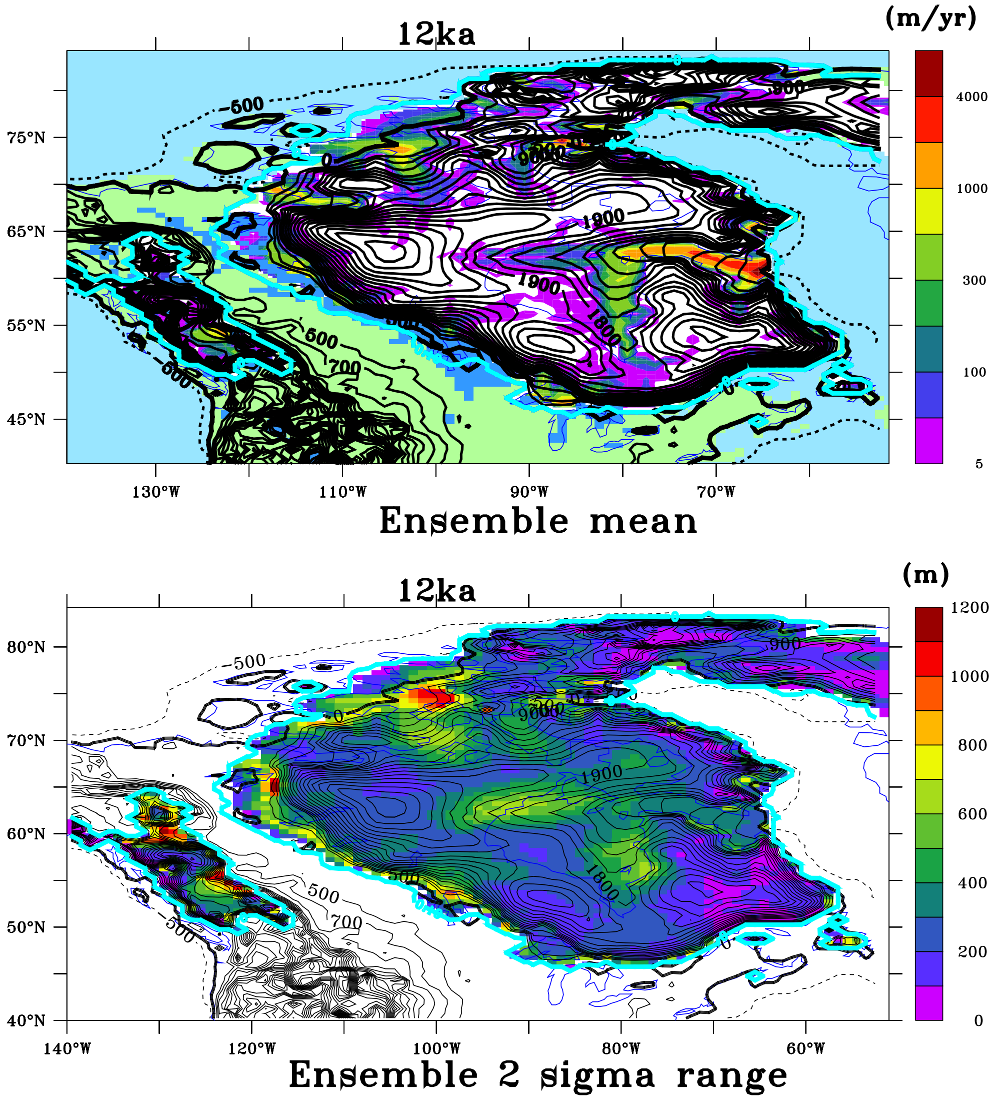

Figure .11: 12 ka weighted mean basal velocity and surface elevation for ensemble N5a and (one-way) two sigma range for ice thickness.

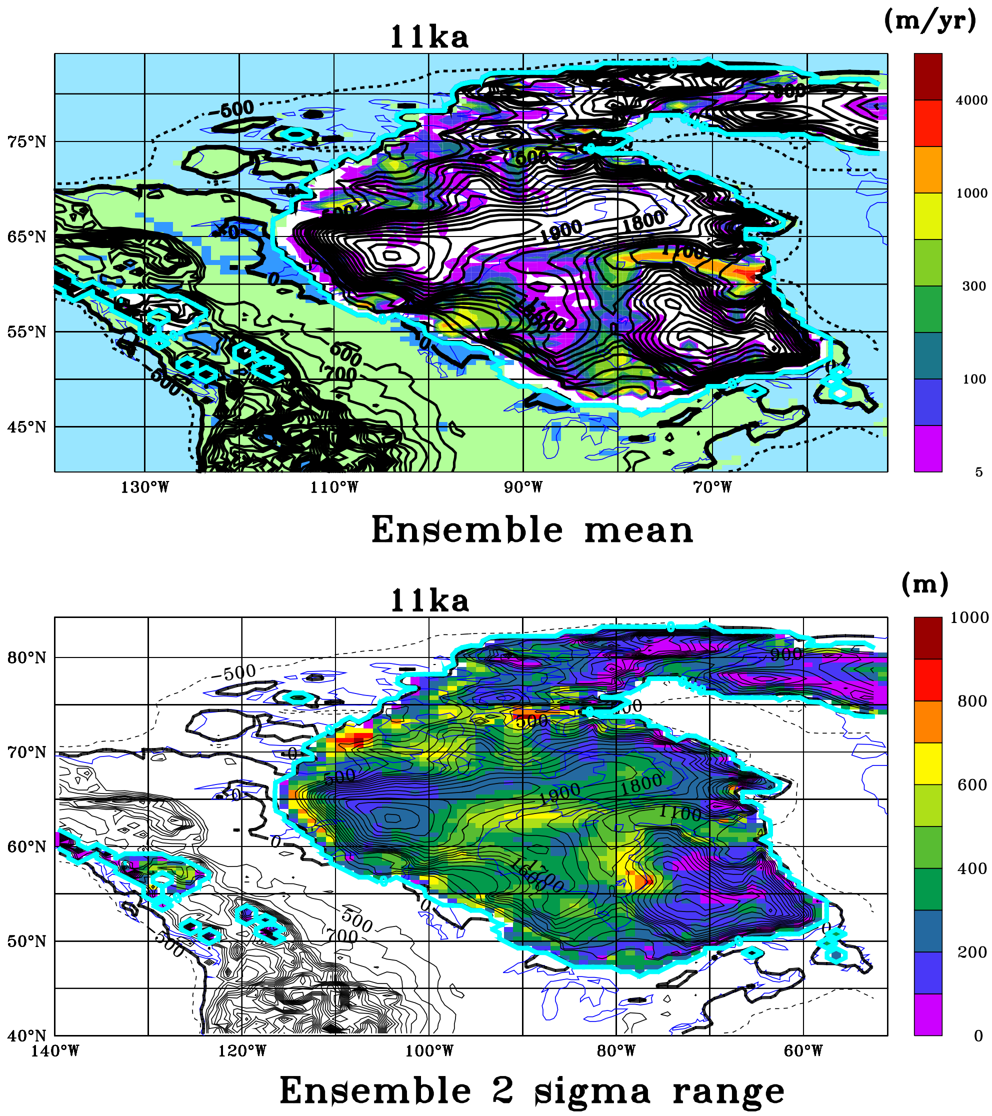

Figure .12: 11 ka weighted mean basal velocity and surface elevation for ensemble N5a and (one-way) two sigma range for ice thickness.

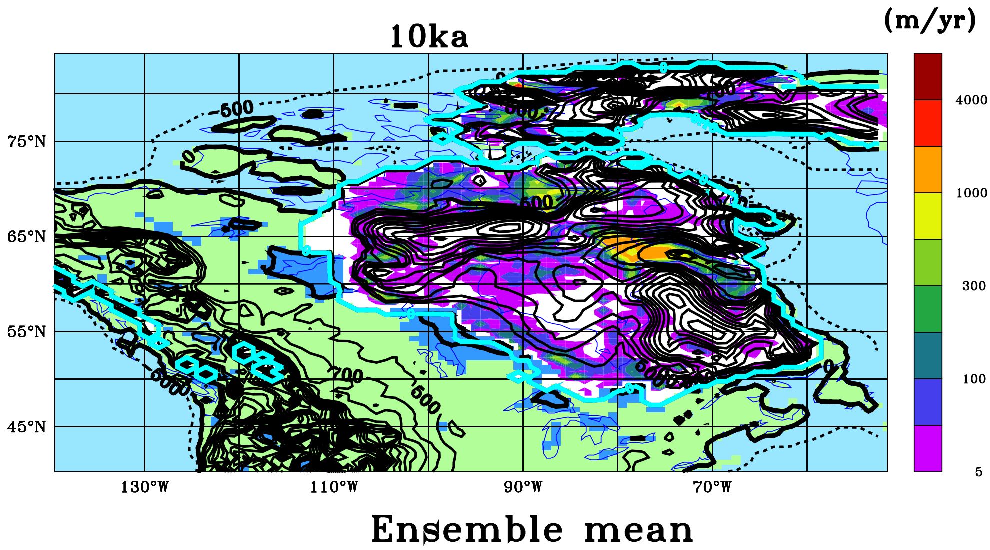

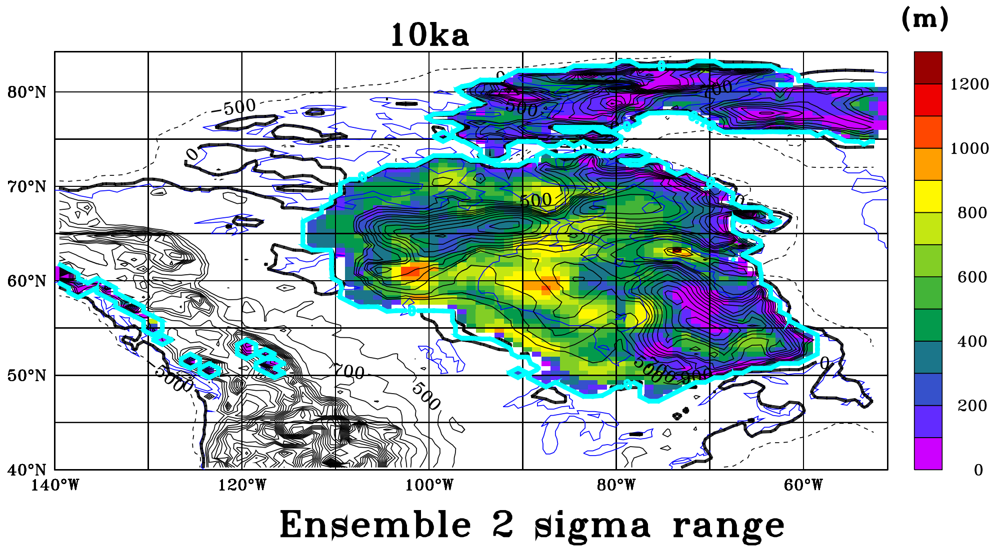

Figure .13: 10 ka weighted mean basal velocity and surface elevation for ensemble N5a and (one-way) two sigma range for ice thickness.

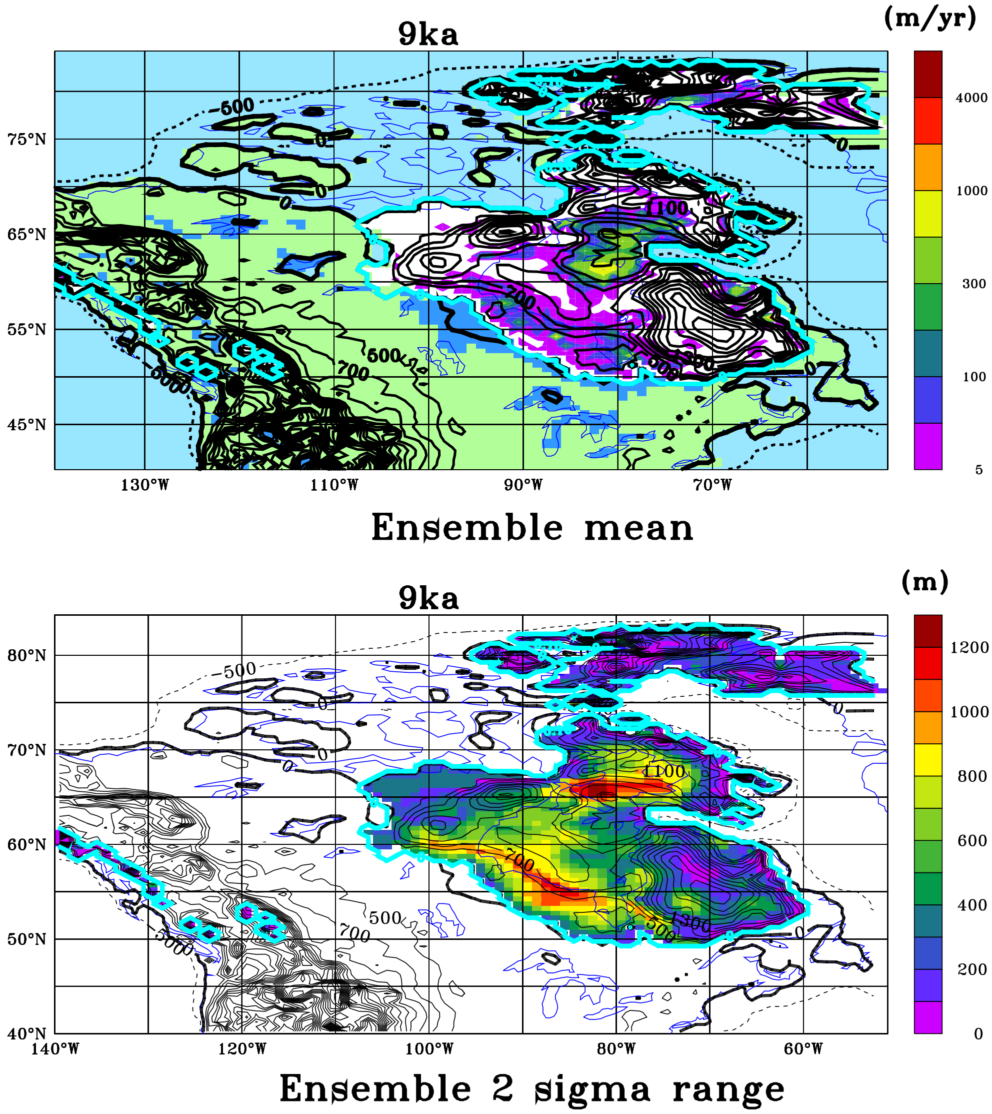

Figure .14: 9 ka weighted mean basal velocity and surface elevation for ensemble N5a and (one-way) two sigma range for ice thickness.

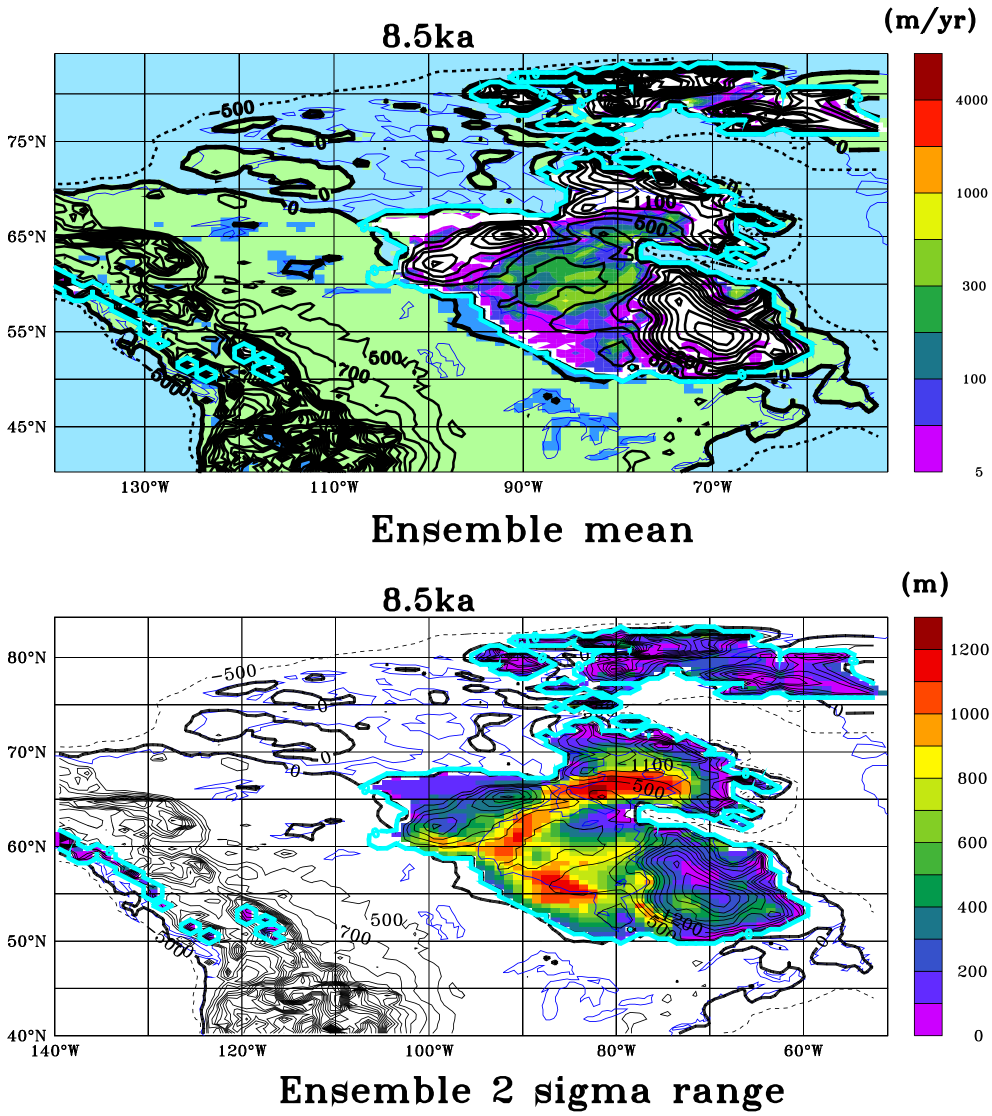

Figure .15: 8.5 ka weighted mean basal velocity and surface elevation for ensemble N5a and (one-way) two sigma range for ice thickness.

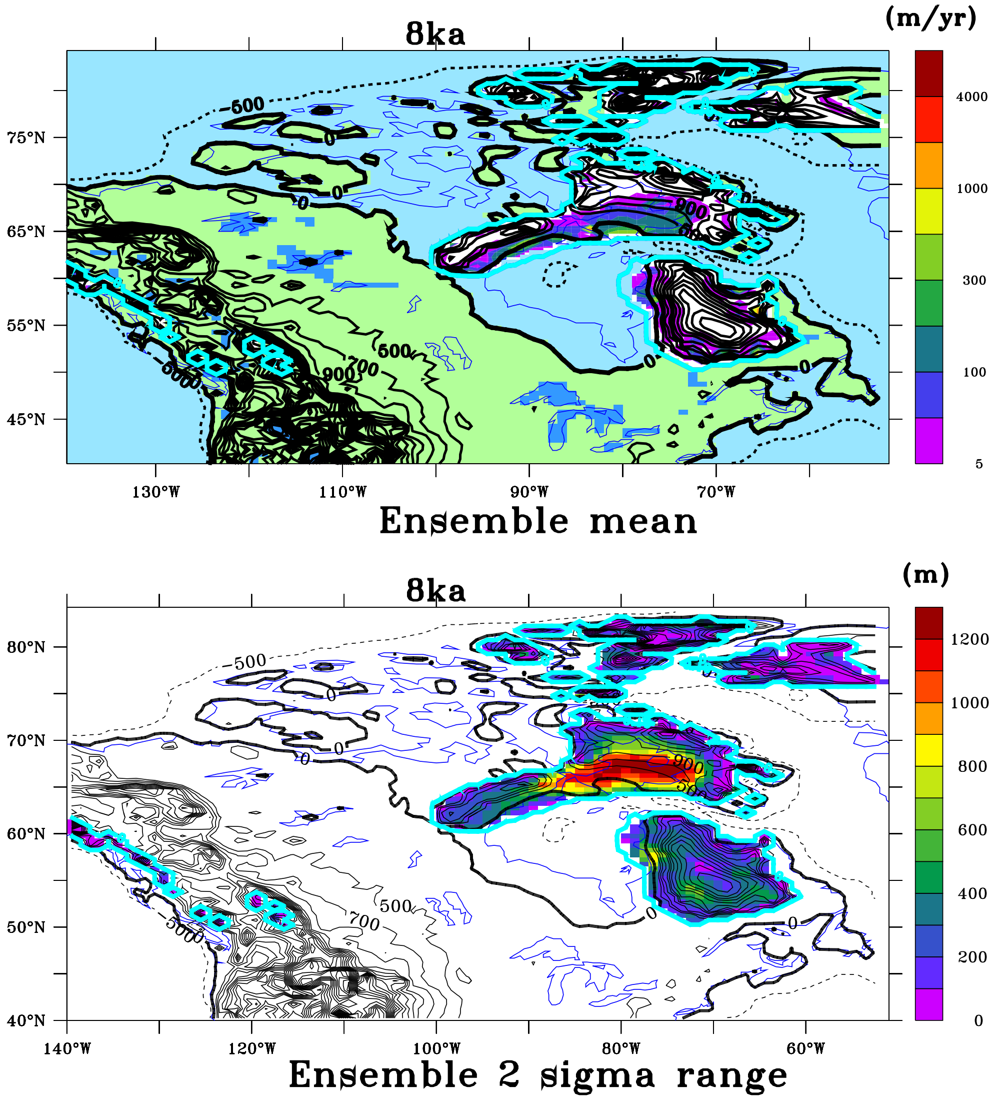

Figure .16: 8 ka weighted mean basal velocity and surface elevation for ensemble N5a and (one-way) two sigma range for ice thickness.

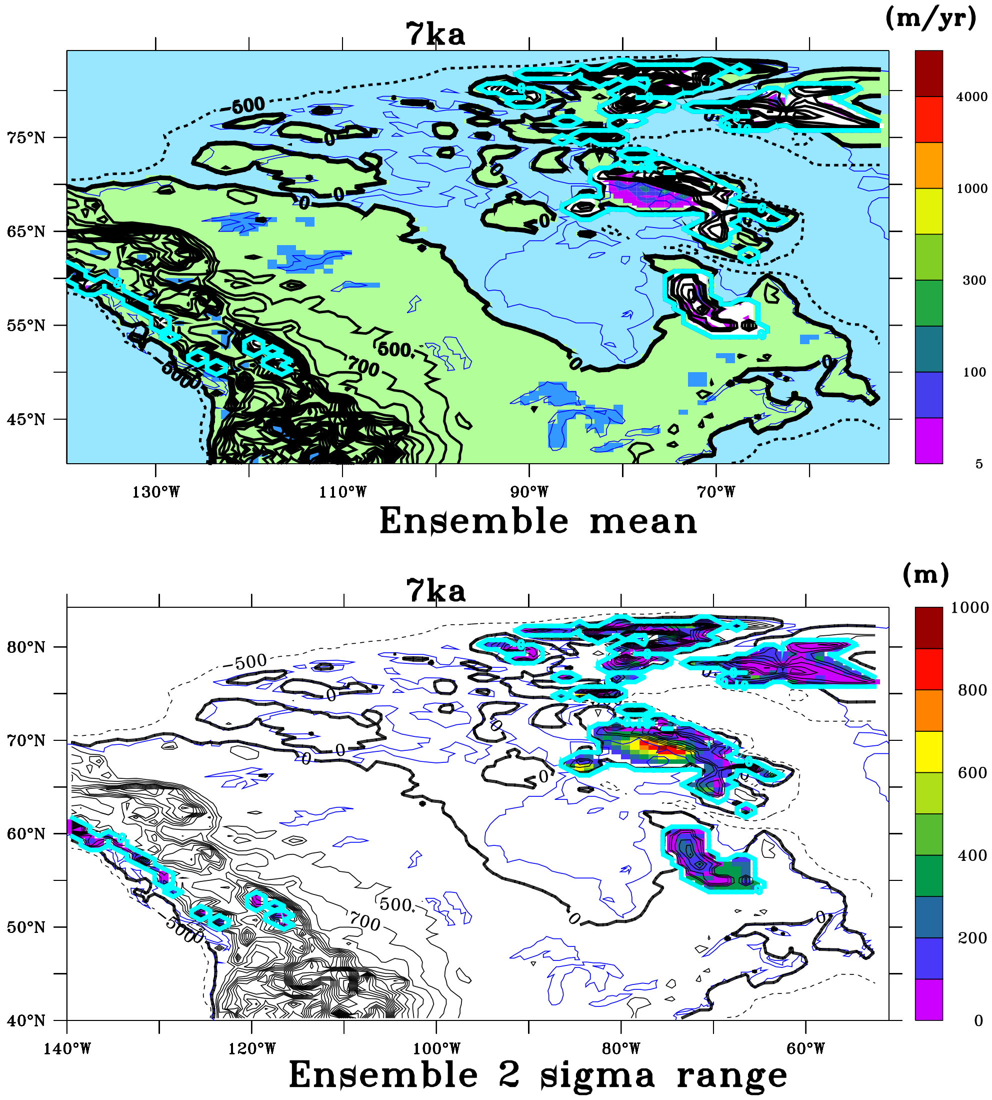

Figure .17: 7 ka weighted mean basal velocity and surface elevation for ensemble N5a and (one-way) two sigma range for ice thickness.

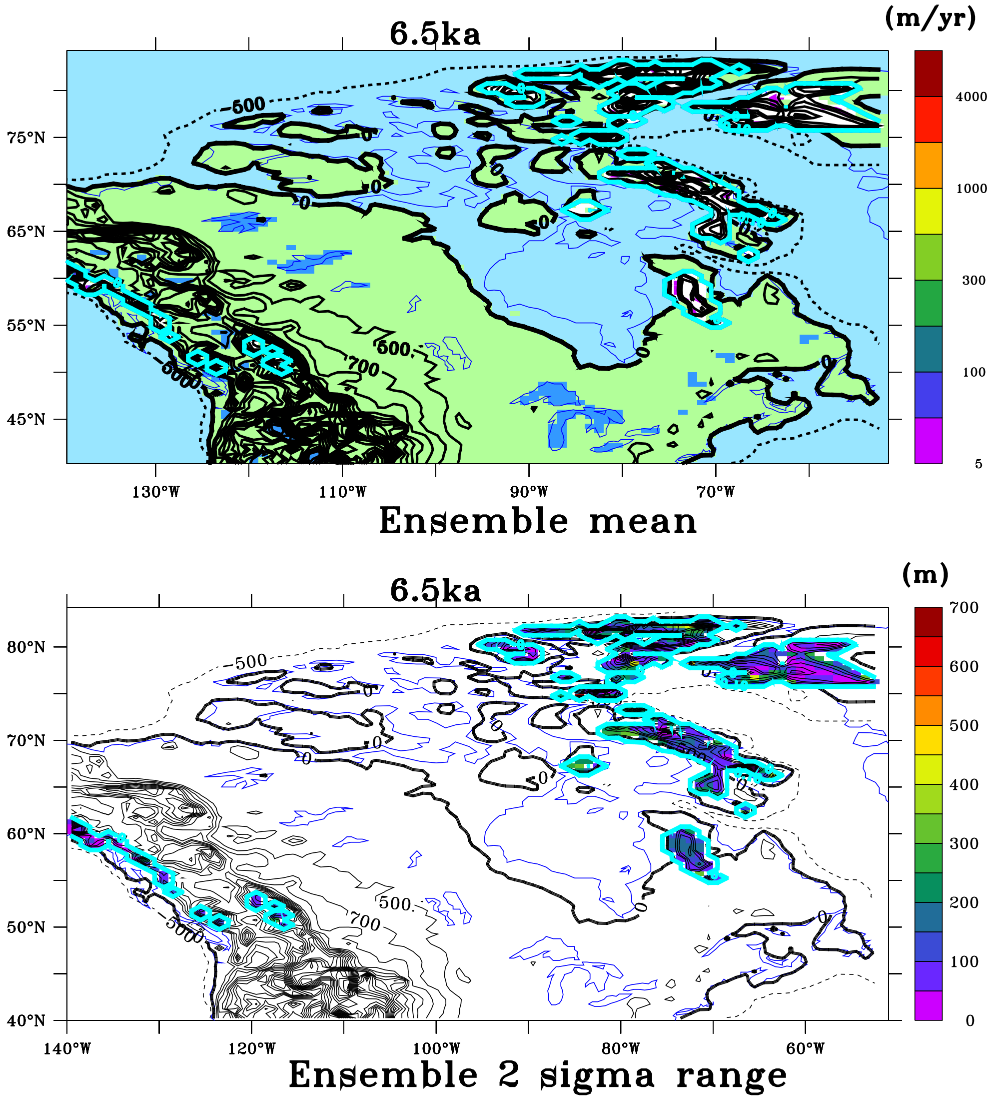

Figure .18: 6.5 ka weighted mean basal velocity and surface elevation for ensemble N5a and (one-way) two sigma range for ice thickness.